ResearchGate

See discussions, stats, and author profiles for this publication at: https://www.researchgate.net/publication/260147806

Fragmentation Dynamics of Doubly Charged Methionine in the Gas Phase

ARTICLE *in* THE JOURNAL OF PHYSICAL CHEMISTRY A · FEBRUARY 2014

Impact Factor: 2.69 · DOI: 10.1021/jp4113238 · Source: PubMed

CITATIONS
6

READS
34

9 AUTHORS, INCLUDING:

Eero Itälä
University of Turku
19 PUBLICATIONS **77** CITATIONS
SEE PROFILE

Kuno Kooser
University of Turku
49 PUBLICATIONS **157** CITATIONS
SEE PROFILE

Samuli Urpelainen
Lund University
52 PUBLICATIONS **213** CITATIONS
SEE PROFILE

Edwin Kukk
University of Turku
228 PUBLICATIONS **2,799** CITATIONS
SEE PROFILE

Available from: Edwin Kukk
Retrieved on: 27 January 2016

THE JOURNAL OF PHYSICAL CHEMISTRY A

Article

pubs.acs.org/JPCA

Fragmentation Dynamics of Doubly Charged Methionine in the Gas Phase

Dang Trinh Ha,*[,†] Y. Wang,[‡,§] M. Alcamí,[‡] E. Itälä,[†] K. Kooser,[†] S. Urpelainen,[∥,⊥] M. A. Huels,[¶,#] E. Kukk,[†] and F. Martín[‡,§]

[†]Department of Physics and Astronomy, University of Turku, FIN-20014 Turku, Finland

[‡]Departamento de Química, Módulo 13, Universidad Autónoma de Madrid, 28049 Madrid, Spain

[§]Instituto Madrileño de Estudios Avanzados en Nanociencia, Cantoblanco, 28049 Madrid, Spain

[∥]Department of Physics, University of Oulu, FIN-90014 Oulu, Finland

[⊥]MAX IV Laboratory, Lund University, P.O. Box 118, SE-22100 Lund, Sweden

[¶]Department of Nuclear Medicine and Radiobiology, Faculty of Medicine, University of Sherbrooke, J1K 2R1 Sherbrooke, Quebec, Canada

[#]Atomic and Molecular Physics, Royal Institute of Technology KTH, SE-10044 Stockholm, Sweden

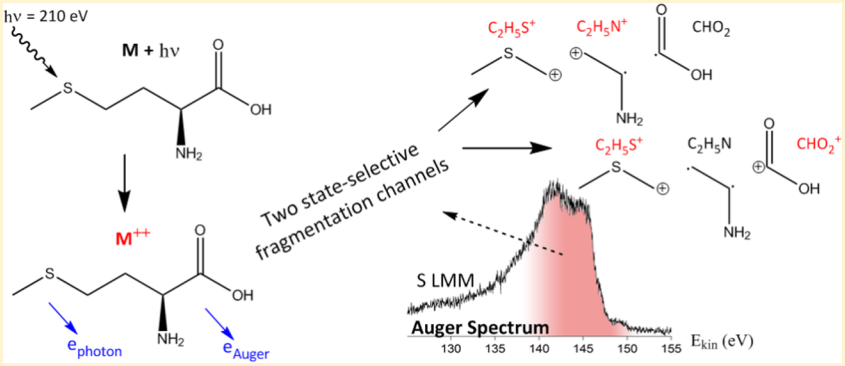

ABSTRACT: The dependence of the fragmentation of doubly charged gas-phase methionine ($C_5H_{11}NO_2S$) on the electronic-state character of the parent ion is studied experimentally by energy-resolved electron ion−ion coincidence spectroscopy. The parent dication electronic states are populated by Auger transitions following site-specific sulfur 2p core ionization. Two fragmentation channels are observed to be strongly dependent on the electronic states with vacancies in weakly bound molecular orbitals. All-electron calculations are applied to assign doubly charged final states of sulfur 2p core ionized methionine. In addition, the Car−Parrinello method is applied to model fragmentation dynamics of doubly charged methionine molecules with various initial temperatures to understand the typical characteristics of the molecular dissociation and partly to support the interpretation of experimental data.

INTRODUCTION

Research on dissociation of biomolecules induced by soft X-ray radiation is of great interest, because it provides not only fundamental knowledge on molecular fragmentation mechanisms but also vital information aiding comprehension of biological damage inflicted by radiation. Biomolecule methionine ($C_5H_{11}NO_2S$) is an essential amino acid (Figure 1) which is not produced by our bodies but plays an important role in metabolism. It is a primary source of sulfur in the live body and an intermediate in the formation of many other essential amino acids; if improperly converted, it can lead to disease.[1] The interaction of soft X-ray radiation and organic molecules tends to inflict damage resulting in ultrafast molecular fragmentation, which may govern the effects of neighboring molecules. Studying isolated methionine molecules provides detailed information about the fundamental dissociation processes induced by radiation, which is essential knowledge before investigating radiation damage on any bigger systems such as proteins.

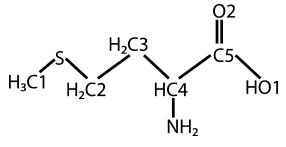

Figure 1. Simplified molecular geometry of methionine with carbon and oxygen atoms enumerated.

Received: November 18, 2013
Revised: January 29, 2014
Published: February 11, 2014

ACS Publications © 2014 American Chemical Society

For studying molecular fragmentation and dynamics,[2−6] energy-resolved electron ion ion coincidence techniques are well established as an excellent experimental tool, particularly in combination with synchrotron radiation excitation. Theoretical modeling of photoresponse of molecules to X-rays has also made significant progress and more detailed and direct comparisons with experiment have become possible.

In this research we study state-selective fragmentation of doubly charged methionine molecules experimentally by recording coincidences of energy-resolved Auger electrons with two singly charged cation fragments from the parent dicationic state. Ab initio methods were also applied to aid interpreting the experimental data. The particular type of coincidence experiment has been referred to in literature (e.g., ref 7) by the acronym of AEPIPICO (Auger electron photoion photoion coincidence), which we will also adhere to in this text.

Methionine, being a rather small molecule, offers a diverse but not overly complex molecular orbital structure for inspection. The presence of a single S atom is also essential for this study, because it allows us to create a well-defined initial core−hole state in a particular atomic site (as the S 2p ionization energy is lower than that of other core orbitals in the molecule, with appropriate choice of photon energy other core ionizations can be excluded). Auger transitions fill the S 2p vacancies and create the dicationic states of the parent molecule, defining the starting conditions for the dissociation. Resolving Auger electron energy (that is defined by the location of the two vacancies at various MOs in the Auger final state) in the AEPIPICO measurement allows us to link specific sets of dissociation pathways (ion−ion coincidences) with particular dicationic electronic states.

In a few cases fragmentation dynamics cannot be explicitly derived from experimental data, e.g., because of possible overlaps where different dissociation channels result in the same mass-to-charge ratios (m/z). Ab initio molecular dynamics (MD) calculations with conditions set by the experiments provide detailed insight into the fragmentation dynamics, which can be contrasted with the experimental results and also be used for interpreting experimental data. The ab initio MD calculations in this work were performed by using Car−Parrinello (CP) MD[8] implemented in the CPMD code.[9] The CP MD method offers a tool for simulating nuclear motions of doubly charged methionine molecules in the ground state accurately and fast. However, the method does not enable performing molecular dynamics starting from the Auger final states as, e.g., the time-dependent density functional theory Ehrenfest-MD (TDDFT-EMD) method[10−13] does. In this sense, it is desirable to compensate the relaxation energies of doubly charged methionine molecules from the Auger final states to the ground state by adding various initial temperatures to the CP MD simulations. The procedure demonstrates to what extent the CP MD method is capable of validly describing fragmentation of doubly charged methionine molecules and also gives an idea of typical characteristics of the fragmentation dynamics of the same molecules, which renders another aspect on the current research in addition to the experimental method.

COMPUTATIONAL METHODS

Auger Electron Spectrum Simulation. The theoretical kinetic energies of the Auger electrons in this research were estimated by means of all-electron calculations, which is presented, e.g., in the thesis of López-Tarifa.[14] In short, the energy released by an electron from orbital j decaying to a core orbital (S 2p) is given by

$$E^{j}_{\mathrm{decay}} = E^{j} - E^{\mathrm{core}}$$

where E^{j} and E^{core} are energies related to orbital j and a core orbital, respectively. The ionization energy needed for a secondary electron from orbital i is estimated by

$$E^{i}_{\mathrm{ioniz}} = E^{\mathrm{HOMO}} - E^{i} + \mathrm{IP2}$$

where E^{HOMO} and E^{i} are energies related to the highest occupied molecular orbital (HOMO) and orbital i. The second ionization potential IP2 is estimated by taking the absolute value of the difference of the total energies of singly and doubly charged methionine. (In this simple model, we made a rough approximation by defining Auger electron's ionization energy by using the singly charged methionine in its ground state but not in the excited state.) Thus, when the condition $E^{j}_{\mathrm{decay}} > E^{i}_{\mathrm{ioniz}}$ is met, the Auger process occurs, and the possible values of kinetic energies for Auger electron ionized from an orbital i enabled by the energy release E^{j}_{decay} in electron decaying from an orbital j are

$$E^{ij} = E^{j}_{\mathrm{decay}} - E^{i}_{\mathrm{ioniz}}\,, \qquad E^{j}_{\mathrm{decay}} > E^{i}_{\mathrm{ioniz}}$$

The energies of the Kohn−Sham (KS) orbitals needed for the theoretical Auger lines were sampled from the molecular structures computed by using the GAUSSIAN 03 package[15] at the level of BLYP/6-311++G(3df,2pd)//BLYP/6-311+G(d,p).

Molecular Dynamics. As the CP MD method allows modeling molecular systems only in their ground states, the energies compensating for the relaxation of the Auger final states are taken into account by adding various initial temperatures. The compensating temperatures were estimated according to the KS orbital energy difference between the doubly vacant HOMO and the two inner orbitals where the vacancies are created after Auger emission, which is added to the experimental temperature (433 K). Here, various initial temperatures ranging from 3630 to 19896 K were added to the CP MD simulations in the microcanonical (NVE) ensemble starting from the last atomic structure of an equilibrated CP MD trajectory of 5 ps in the canonical (NVT) ensemble. The gradient-corrected exchange−correlation functional of Becke, Lee, Yang, and Parr (BLYP) was used in the calculations. The Coulomb potential of core electron−nucleus interaction was replaced by the Kleinman−Bylander pseudopotentials,[16] and a plane wave basis set with an energy cutoff of 70 Ry was used for describing the valence electrons. The lengths of a cubic box associated with the plane wave basis functions were chosen to be L = 3 nm for the temperatures T = 12174 K, T = 13198 K, and T = 15292 K, and L = 2 nm for the remaining temperatures. The time step of 24 as and the fictitious electronic mass of 100 u were applied in all simulations. The atomic charges along the CP MD trajectories were obtained by using Bader's charge analysis.[17,18]

EXPERIMENTAL METHODS

The experiments were performed at the undulator-based soft X-ray beamline I411 at the MAX-II synchrotron radiation source (Lund University, Sweden).[19] The undulator radiation was monochromatized by a Zeiss SX-700 plane-grating monochromator.

The apparatus used for the present coincidence experiments is described in detail elsewhere.[20] Briefly, the apparatus consists

dx.doi.org/10.1021/jp4113238 | J. Phys. Chem. A 2014, 118, 1374−1383

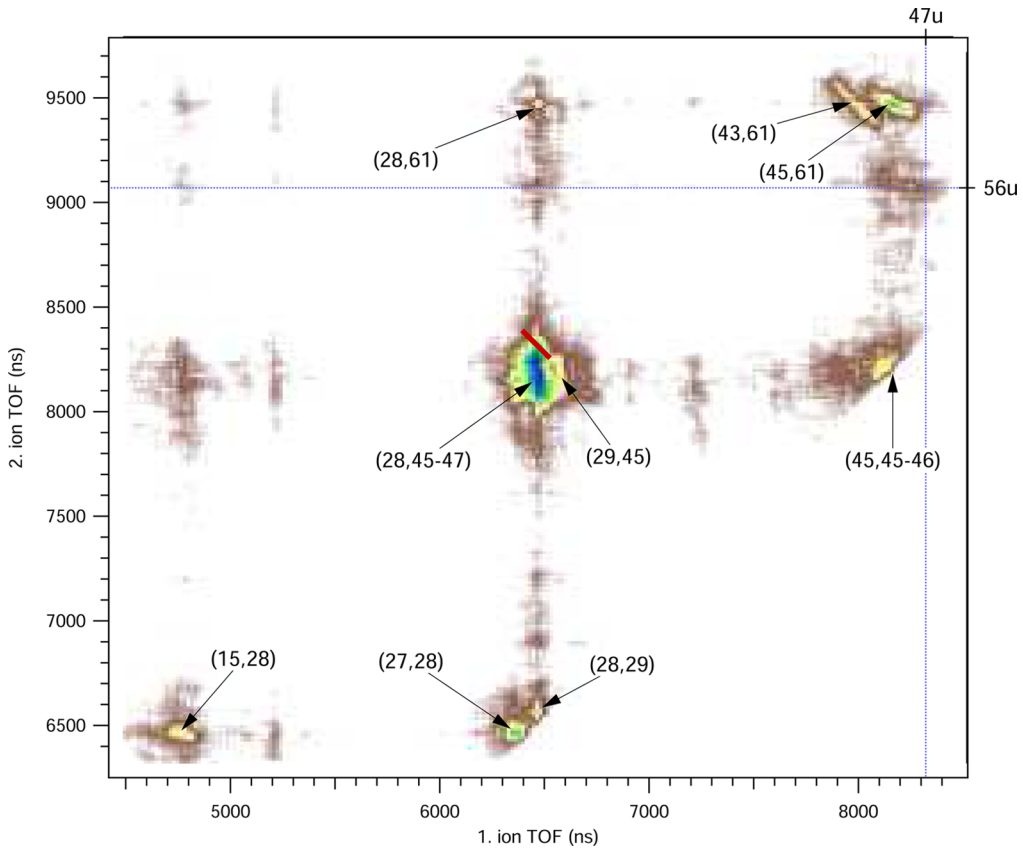

Figure 2. AEPIPICO map of methionine from coincidence measurements with S LMM Auger electrons. Labels refer to the mass pairs of the detected ion pairs. The red, short diagonal line on the (28,47) pattern illustrates a possible slope of −1. The crossing of two dotted lines corresponds to the ion pair (47,56) predicted in a CP MD result.

of a homemade Wiley−McLaren type ion time-of-flight (TOF) detector with a 400 mm long drift tube and a modified Scienta SES-100 electron energy analyzer.[21] The original CCD camera of the electron spectrometer was replaced by a resistive anode detector. The TOF spectrometer is equipped with a 70 mm Hamamatsu microchannel plate (MCP) detector. The ion detection electronics is based on a 1 GHz waveform digitizer card (Signatec PDA 1000). The AEPIPICO measurements were performed in pulsed-field mode, where the detection of electrons by the electron analyzer triggers the extraction field for ions. The used extraction and acceleration voltages are 160 and 885 V, respectively.

The recorded signals of an electron and the ions from the same event are so-called true coincidences. In contrast, false coincidences are such events where the ion TOF spectrometer detects one or more fragments from a different molecule than the one emitting the detected electron. The false/true coincidence ratio was kept at a minimum by using low count rates of about 10 electrons/s. In addition, a pulse generator was used during the AEPIPICO measurements to provide non-coincident extraction pulses at a constant frequency. The signals of ion−ion coincidences were thus initially triggered in two different ways (by electrons and by pulse generator) and were collected simultaneously. The average number of ions per electron trigger and the number of ions per artificial trigger (including detector noise counts) were, respectively, 0.99 and 0.67. The acquired data were analyzed with the help of custom-made IGOR PRO software based data analysis macros.[22] In the present experiment, Auger electrons were measured in coincidence with positive ionic fragments, and m/z's of the cationic fragments were determined by their flight time in the TOF tube. The ion TOFs were converted to m/z ratios by using the formula $m/z = (\mathrm{TOF} - T_0)^2/C^2$, where the used calibration parameters were $T_0 = 159$ ns and $C = 1190.62$ ns $(e/u)^{1/2}$.

In addition to the methionine sample, measurements were also performed on isotopically labeled methionine, where the carbon in carboxyl group is replaced by ^{13}C. The methionine samples were purchased from Sigma-Aldrich with purity greater than 99%. During the measurements, the samples were evaporated into the sample area using an effusion cell (MBE Komponenten NTEZ40 oven) at the temperature of 160 °C. The photon energy used for the AEPIPICO measurements was $h\nu = 210$ eV to ionize S 2p photoelectrons with the photon bandwidth of 400 meV. This energy is about 40 eV above the S 2p ionization edge. The Auger electron kinetic energy window was set to be from 125 to 155 eV for recording Auger electron spectrum and from 127 to 151 eV for recording Auger electrons in the AEPIPICO measurements. The entrance slit of the electron spectrometer was 0.8 mm and the pass energy 200 eV, which corresponds to the electron energy resolution of 640 meV. During the experiments, the chamber pressure was in the 10^{-7} mbar range.

RESULTS AND DISCUSSION

Overview. After photoionization of an electron from the inner 2p shell of the sulfur atom in methionine, an Auger electron is emitted via a relaxation process resulting in a doubly charged molecule. Auger transitions typically create molecules

dx.doi.org/10.1021/jp4113238 | J. Phys. Chem. A 2014, 118, 1374−1383

Table 1. List of Fragmentation Products Based on the Mass-to-Charge Ratios Acquired from the AEPIPICO Measurement at 210 eV Photon Energy (Left Side: Cationic Fragments. Right Side: Neutral Fragments)

fragment 1	m/z	m/z	frag 2	frag 3	frag 4	frag 5	frag 6
CH_3^+	15	28	$(CH_2)_2^+$	$CHNH_2COOH$	S		
CH_3^+	15	28	CH_2N^+	$S(CH_2)_2$	COOH	H	
NH^+	15	28	$(CH_2)_2^+$	CHCOOH	MeS	H	
$CHCH_2^+$	27	28	CH_2N^+	MeS	COOH	H	H
CHN^+	27	28	$(CH_2)_2^+$	MeS	COOH	H	H
$(CH_2)_2^+$	28	45	$COOH^+$	MeS	$CHNH_2$		
CH_2N^+	28	45	$COOH^+$	$MeS(CH_2)_2$	H		
$(CH_2)_2^+$	28	46−47	$CH_{n=2,3}S^+$	$CHNH_2COOH$	$H \times (3 - n)$		
CH_2N^+	28	46−47	$CH_{n=2,3}S^+$	$(CH_2)_2$	$H \times (4 - n)$	COOH	
$CHNH_2^+$	29	45	$COOH^+$	$MeS(CH_2)_2$			
$CH_2CHNH_2^+$	43	61	$MeSCH_2^+$	COOH			
$COOH^+$	45	45−46	$CH_{n=1,2}S^+$	$(CH_2)_2CHNH_2$	$H_{n=2,1}$		
$COOH^+$	45	61	$MeSCH_2^+$	CH_2CHNH_2			

with high internal energy that have a high probability to dissociate via various multibody fragmentation mechanisms.[23] Before presenting the results for methionine molecule, let us classify the various fragmentation scenarios. First, two-body dissociation following Auger decay of core hole states has been a very minor channel in other organic molecules[24] or has not been observed at all.[25] This is also the case for methionine, as will be seen later. Instead, three- and four-body channels are observed, or even larger number of fragments. Three-body dissociation mechanisms can be divided into three categories:

- **Type I:** *Deferred charge separation*, where charge separation occurs after ejection of a neutral fragment,

$$ABC^{++} \rightarrow A + BC^{++}$$

$$BC^{++} \rightarrow B^+ + C^+$$

- **Type II:** *Secondary dissociation*, where charge separation occurs prior to ejection of a neutral fragment,

$$ABC^{++} \rightarrow AB^+ + C^+$$

$$AB^+ \rightarrow A + B^+$$

- **Type III:** *Concerted dissociation*, where all fragments are released simultaneously,

$$ABC^{++} \rightarrow A + B^+ + C^+$$

In the majority of dicationic dissociation, charge separation occurs and two singly charged fragments (plus neutral ones) are produced. Plotting the flight time of the slower (heavier) cation fragment versus the faster one forms a 2D TOF correlation map, a so-called photoion photoion coincidence (PIPICO) map, where patterns correspond to various momentum-correlated cation pairs. Depending on the type of process, the kinematics of the process and the orientational distribution of the dissociating molecules, these patterns can have various lengths, widths and slopes. Blurring of the patterns occurs due to the presence of neutral ("dark") fragments, reducing the momentum correlation of the ions. The patterns close to the diagonal (that occur with ion pairs with the same m/z) are incomplete, due to the deadtime effects that in our case prevented detecting ions arriving less than 30 ns apart.

Fragmentation Channels. Before investigating the state-dependency of fragmentation, let us consider the identification of various m/z pairs as specific fragmentation channels. Because all detected ions in this experiment were singly charged, we will refer to the ions only by their mass, given in atomic mass units. An AEPIPICO map of methionine fragment ions detected in coincidence with S LMM Auger electrons (within the 127−151 eV energy window) is shown in Figure 2.

The main observed cation pairs are listed in Table 1 together with their possible assignments as fragmentation channels. Next we investigate these assignments in detail. The assignment of cationic fragments was made with the assumption that no rearrangement of the heavier atoms (C, O, N, S) takes place prior to the fragment separation. Measurements were also performed on a sample where the carbon in the carboxyl group was replaced by ^{13}C. These results were used to exclude some fragmentation products and pathways from Table 1 as explained next.

The heaviest observed ion pairs are at m/z pairs (43,61) and (45,61). Their assignment to fragmentation channels is quite straightforward, if simple bond scissoring model is assumed (Figure 3a,b). Both correspond to the same bond scissoring

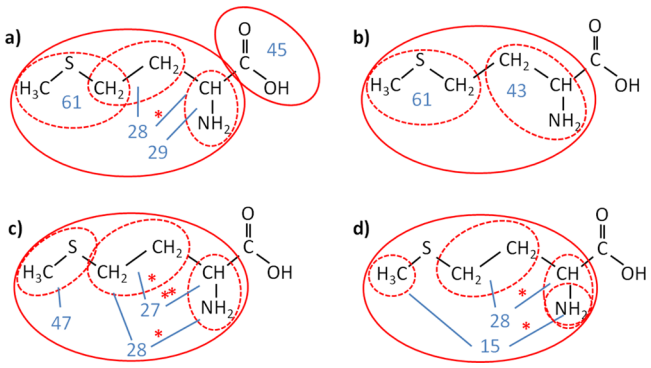

Figure 3. Dissociation channels for methionine. Solid circles: charged fragments after primary stage. Dashed circles: secondary dissociation charged fragments. Stars mark hydrogen loss and numbers fragment masses.

sites, but with different charge localization. In Figure 2 the m/z pair (43,61) has a well-defined momentum-correlated shape with the slope of −1. The fragmentation dynamics producing this ion pair is therefore clearly deferred charge separation (Type I) where low-kinetic-energy neutral fragment COOH is ejected prior to charge separation into $CH_2CHNH_2^+$ and $MeSCH_2^+$ (Figure 3b):

dx.doi.org/10.1021/jp4113238 | J. Phys. Chem. A 2014, 118, 1374−1383

(i) $MeS(CH_2)_2CH(NH_2)COOH^{2+}$
$\rightarrow MeS(CH_2)_2CHNH_2^{2+} + COOH \rightarrow$

(ii) $MeS(CH_2)_2CHNH_2^{2+} \rightarrow MeSCH_2^+ + CH_2CHNH_2^+$

Based on the length of the pattern (294 ns), the estimated maximum kinetic energy release (KER) in the deferred charge separation phase is 3.4 ± 0.5 eV, as determined by the assumption that the kinetic energy release is minimal in the primary process and the momentum correlation in the charge separation process is partially preserved.

The m/z pair (45,61) in Figure 2 is quite unambiguously assigned to the $COOH^+$ and $MeSCH_2^+$ cations (Figure 3a), and the corresponding pattern in the isotopic substitution measurement results is, in fact, shifted to m/z pair (46,61). The slope of −0.6 of the pattern matches perfectly with the theoretical value of $k = -0.59$ derived from a secondary dissociation fragmentation process of Type II:

(i) $MeS(CH_2)_2CH(NH_2)COOH^{2+}$
$\rightarrow MeS(CH_2)_2CHNH_2^+ + COOH^+ \rightarrow$

(ii) $MeS(CH_2)_2CHNH_2^+ \rightarrow MeSCH_2^+ + CH_2CHNH_2$

where the lighter cation $COOH^+$ is released in the primary step and the heavier cation $MeSCH_2^+$ in the secondary step. The estimated maximum KER into cation fragments is 2.3 ± 0.5 eV from the pattern length of 227 ns, again, as determined by assuming the kinetic energy release to be dominant only in the charge separation phase. The nuclear dynamics of both m/z pairs (43,61) and (45,61) channels are thus quite similar, the carboxyl radical separating in the first phase and the remaining molecule breaking at the $-CH_2-CH_2-$ bond in the second. The difference is in charge localization.

There is a weak pattern in Figure 2 corresponding to m/z pairs (45,45−46). The pattern is blurred and clipped due to being at the diagonal, and thus the fragmentation dynamics cannot be analyzed from the slope or KER. The most probable fragments related to these pairs are ($COOH^+$, $CH_{n=1,2}S^+$).

The carboxyl ion (m/z 45, m/z 46 after ^{13}C substitution) is seen to form coincident pairs also with lighter ions. The most intense pattern in Figure 2 has a large and irregular shape and corresponds to several m/z pairs (28,45−47) and (29,45). This pattern is shifted upward upon ^{13}C substitution. The overlapping patterns makes slope analysis inaccurate; however, these patterns clearly have a very steep slope suggesting that the dissociation process is again of Type II. For the m/z pair (29,45):

(i) $MeS(CH_2)_2CH(NH_2)COOH^{2+}$
$\rightarrow MeS(CH_2)_2CHNH_2^+ + COOH^+ \rightarrow$

(ii) $MeS(CH_2)_2CHNH_2^+ \rightarrow MeS(CH_2)_2 + CHNH_2^+$

where the stable carboxyl cation (m/z 45) is produced in the primary step and the lighter cation $CHNH_2^+$ (m/z 29) in the secondary step. This channel is again described by Figure 3a, where the scissoring in the secondary dissociation now occurs at the $-CH_2-CH-$ bond. Note that because the heavier of the two detected ions is released in the first step (vs in the second step for the m/z pair (45,61)), the slope becomes *steeper*.[23,24,26] It is −3.6 in the case where the lighter ion $CHNH_2^+$ is produced in the secondary step, whereas the slope would be −0.4 if the heavier carboxyl ion $COOH^+$ were produced in the secondary step.

The m/z pair (28,45) has several assignments for the lighter ion, but following the above sequence of events, it can be assigned to the channel (CH_2N^+, $COOH^+$). In this case, it is the same process as with the m/z pair (29,45), but accompanied by a hydrogen loss from the cation in the second stage (Figure 3a). Alternatively, it can be the $(CH_2)_2$ group that obtains charge in the second stage dissociation and the ion pair is ($(CH_2)_2^+$, $COOH^+$). In both cases, the $-CH_2-CH-$ bond is broken, but the latter ($(CH_2)_2^+$ ion) requires an additional $S-CH_2$ bond breakage. The carboxyl ion is thus seen to form coincidences in a number of secondary fragments from the remaining part of the molecule.

There is evidence of fragment m/z 47 in coincidence with fragment m/z 28. The pair m/z (28,47) corresponds to various channels listed in Table 1. The ion at m/z 47 is most likely CH_3-S^+, but m/z 28 can be either of the cations $(CH_2)_2^+$ or CH_2N^+. However, the m/z 28 cannot be CO^+ from the carboxyl group, because shifting from m/z 28 to m/z 29 is not observed in the isotopic substitution measurement results. The m/z pair (28,47) can originate from the deferred charge separation following the departure of a neutral carboxyl group (Figure 3c):

(i) $MeS(CH_2)_2CH(NH_2)COOH^{2+}$
$\rightarrow MeS(CH_2)_2CHNH_2^{2+} + COOH \rightarrow$

(ii) $MeS(CH_2)_2CHNH_2^{2+} \rightarrow MeS^+ + (CH_2)_2^+ + CHNH_2$

or

(ii) $MeS(CH_2)_2CHNH_2^{2+} \rightarrow MeS^+ + (CH_2)_2 + CH_2N^+ + H$

Peaks at m/z pairs (28,46−47) (and (45,46)) involve breaking the S−C bond, which is in principle weaker than the C−C bonds if we consider standard bond dissociation energies. However, C−S breaks always appear to occur associated with complex processes where other C−C bonds are also broken.

Table 1 lists two possibilities for the m/z pair (27,28). On the PIPICO map of Figure 2, this pattern is quite close to the diagonal and is not well-defined, most probably because the heavy and/or numerous neutral fragments all but destroy the momentum correlation. Also, the KER into these cations is rather small, making slope determination difficult. The likely scenarios, stemming from the above-described channels, are depicted in Figure 3c. In both cases, two hydrogen losses are expected.

Finally, the lightest ion pair that is clearly observed is at m/z pair (15,28). The lighter ion can be either the methyl cation CH_3^+ or NH^+ ion (Figure 3d). Because this pattern is not shifted by isotopic substitution, the heavier fragment again cannot be CO^+ from the carboxyl group. It is not possible to make a definite assignment in this case. However, it is notable that *all* observed patterns can be explained consistently by one general scenario of nuclear dynamics:

(a) Carboxyl radical separates either carrying charge (Figure 3a) or being neutral (Figure 3b−d). None of the observed patterns indicate secondary dissociation of the cationic carboxyl radical.
(b) The remaining part of the molecule always dissociates further into fragments ranging in size from m/z 61 to m/z 15.

dx.doi.org/10.1021/jp4113238 | J. Phys. Chem. A 2014, 118, 1374−1383

(c) There is the possibility of hydrogen loss or transfer accompanying these processes.

In addition to the discussed patterns, Figure 2 shows some other weak spot-like patterns in coincidence with m/z 28. These are most likely due to false coincidences with molecular nitrogen ions from residual gas that were imperfectly subtracted.

Breaking of the C−C bond between the acidic group and the C_α, resulting in the loss of a neutral COOH radical, has been described as the most favorable breaking process in a previous systematic study concerning several singly charged amino acids.[27] It is also one of the most favorable breaking channels observed in other studies involving doubly charged species.[28] The results of this study are consistent with the ones of the mentioned studies: C_α−C_{acid} group is the weakest C−C bond, and COOH is also a good leaving group either as neutral radical or as singly charged species.

Further fragmentation following the loss of the carboxyl group involves complex mechanisms in which the large amount of energy transferred to the systems can be used to break any bond of the methionine skeleton. Note that in the above discussion all possible C−S and C−C bonds can be broken and the corresponding signals observed (Figure 3), hence it is difficult to associate the breaking patterns directly with the strength of the bonds. The central $-H_2C-CH_2-$ bond remains intact most of the time in the different mechanisms discussed; therefore, the fairly stable ethylene cation $(CH_2)_2^+$ is one of the most intense signals in the spectra. In addition, the $CHNH_2^+$ fragment is involved in some of the most intense peaks observed, which suggests that the C−N bond does not appear to break easily in the fragmentation mechanics of doubly charged methionine molecules.

Auger Electron Spectra and State-Selective Fragmentation. On the PIPICO map of Figure 2 the coincident electron was included implicitly (because only events with an Auger electron recorded in the experimental energy window are counted). Let us now consider explicitly the relationship of the fragmentation channels and the Auger electron spectrum. The measured and simulated Auger electron spectra are shown in Figure 4. The theoretical Auger spectrum in this work is not expected to be highly accurate but is generated in a qualitatively sound manner to understand which orbitals are involved in the detected Auger window. On the other hand, as explained in the Molecular Dynamics section, the fitted theoretical Auger spectrum is useful for the research on fragmentation of doubly charged methionine by using CP MD method. Despite the approximations (such as ignoring excited states and the core hole effect in deriving the energy needed for Auger electron emission), the shape of the simulated Auger spectrum fits quite well with the experimental one.

The AEPIPICO technique allows us to inspect the ion pair production as a function of electron energy. In principle, PIPICO maps can be created for narrow ranges of Auger final states. However, due to limited statistics of ion−ion coincidence events, this is not feasible. More detailed information on major observed ion pairs is extracted by counting the pairs within narrow ranges of electron energies.

Figure 5 shows such *ion pair yields* (PIPIYs) as a function of kinetic energy of Auger electrons determined from the AEPIPICO data. Error bars reflect the statistical uncertainties of pair counting and subtracting false events. Two distinctly different behaviors are observed: The heaviest fragment pairs

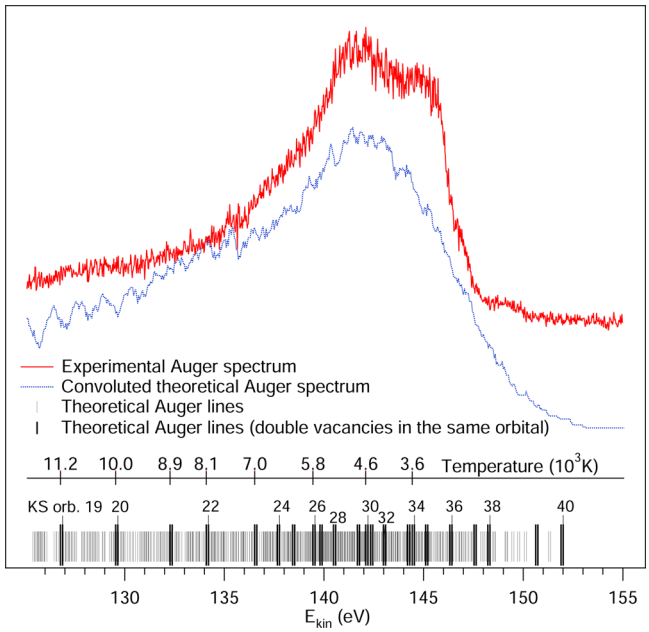

Figure 4. Measured S LMM Auger electron spectrum of methionine (see legend in figure for further details). Gray vertical short bars represent kinetic energies of emitted Auger electrons leaving behind all possible combinations of vacancy orbitals forming different non-equilibrium M^{2+} molecules after S 2p ionizations, whereas long vertical black bars correspond to kinetic energies of emitted Auger electrons resulting in such orbitals where two holes are in the same orbital. The convoluted theoretical Auger spectrum (dashed curve) is a smoothed histogram of the theoretical Auger lines and has been shifted by −15 eV.

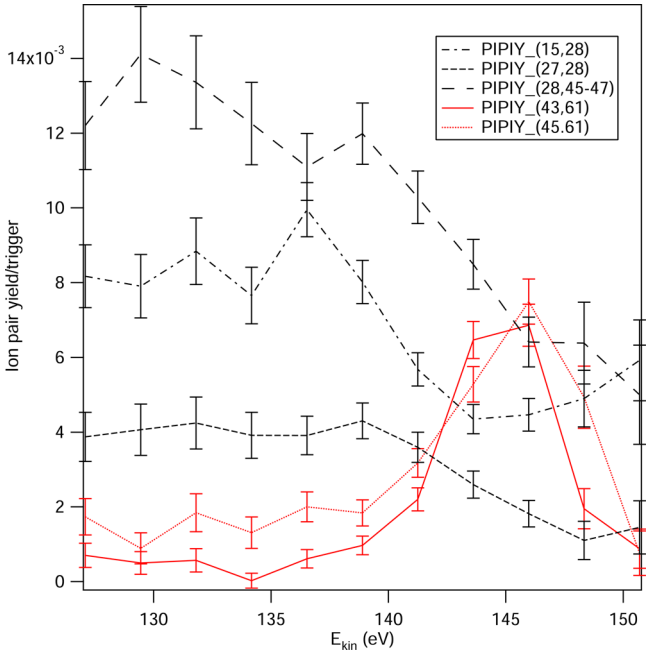

Figure 5. Ion pair yields per Auger electron trigger as a function of electron kinetic energy.

m/z (45,61) ($COOH^+$, $MeSCH_2^+$) and m/z (43,61) ($CH_2CHNH_2^+$, $MeSCH_2^+$) are strongly correlated with the high energy electrons and thus with electronic states having vacancies in HOMOs or outer molecular orbitals. It is also notable that the heavier pair of the two, the m/z pair (45,61),

dx.doi.org/10.1021/jp4113238 | J. Phys. Chem. A 2014, 118, 1374−1383

Table 2. Fragments from CP MD Simulations at Various Temperatures[a]

T (K)	fragments (**u**)^q	broken bonds
3630	$CH_3S(CH_2)_2CH(NH_2)$ (**104**)$^{1.6}$; COOH (**45**)$^{0.4}$	C4−C5
4250	$CH_3S(CH_2)_2CH(NH_2)$ (**104**)$^{1.5}$; COOH (**45**)$^{0.5}$	C4−C5
4632/5327	$CH_3S(CH_2)_2CH(NH_2)$ (**104**)$^{1.8}$; COOH (**45**)$^{0.2}$	C4−C5
5773	$*CH_3SCH_2$ (**61**)$^{0.7}$; COOH (**45**)$^{0.3}$; $*CH_2CH(NH_2)$ (**43**)$^{1.0}$	C2−C3; C4−C5
6210	$*CH_3SCH_2$ (**61**)$^{0.8}$; COOH (**45**)$^{0.2}$; $*CH_2CH(NH_2)$ (**43**)$^{1.0}$	C2−C3; C4−C5
6538	$*CH_3SCH_2$ (**61**)$^{0.8}$; COOH (**45**)$^{0.3}$; $*CH_2CH(NH_2)$ (**43**)$^{0.9}$	C2−C3; C4−C5
7027	$*CH_3SCH_2$ (**61**)$^{1.0}$; COOH (**45**)$^{0.2}$; $*CH_2CH(NH_2)$ (**43**)$^{0.8}$	C2−C3; C4−C5
8072/8854/10026	$*CH_3SCH_2$ (**61**)$^{1.0}$; $*CH_2CH(NH_2)$ (**43**)$^{0.9}$; CO (**28**)$^{0.0}$; OH (**17**)$^{0.1}$	C2−C3; C4−C5; C5−O1
12174	SCH_2 (**46**)$^{0.2}$; $CH_2C(NH_2)$ (**42**)$^{0.8}$; HCO (**29**)$^{0.6}$;[b] OH (**17**)$^{0.0}$; CH_3 (**15**)$^{0.3}$	C1−S; C2−C3; C4−C5; C5−O1
13198	$CH_2CHC(NH_2)$ (**55**)$^{0.9}$; CH_3S (**47**)$^{0.7}$;[c] HCOOH (**46**)$^{0.2}$;[d] H (**1**)$^{0.2}$	S−C2; C3−H1; C4−C5
15292	$*CH_2CHCH(NH_2)$ (**56**)$^{1.0}$; $*CH_3S$ (**47**)$^{0.7}$; COO (**44**)$^{0.2}$; H (**1**)$^{0.1}$; H (**1**)$^{0.0}$	S−C2; C3−H1; C4−C5; O1−H

[a]Stars mark experimentally observed ion pairs. The notation (**u**)^q indicates the mass (**u**) and the calculated charge (q) of the fragment. Charges above (below) +0.5 are likely associated to singly-charged (neutral) fragments (see ref 13 for details). [b]C5 captures H from C4. [c]H transfers from C1 to S. [d]C5 captures H from C4.

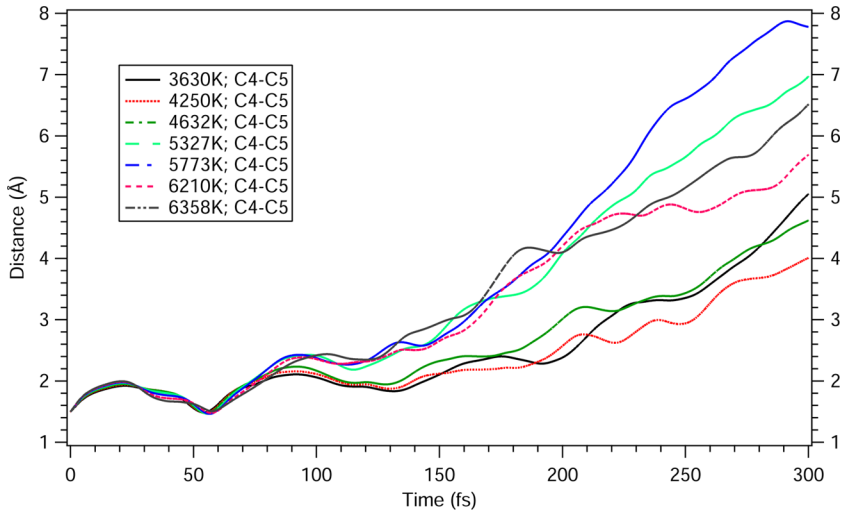

Figure 6. Distances between carbon C4 and C5 in CP MD simulations of doubly charged methionine with various initial temperatures. See legends in the figure for further details.

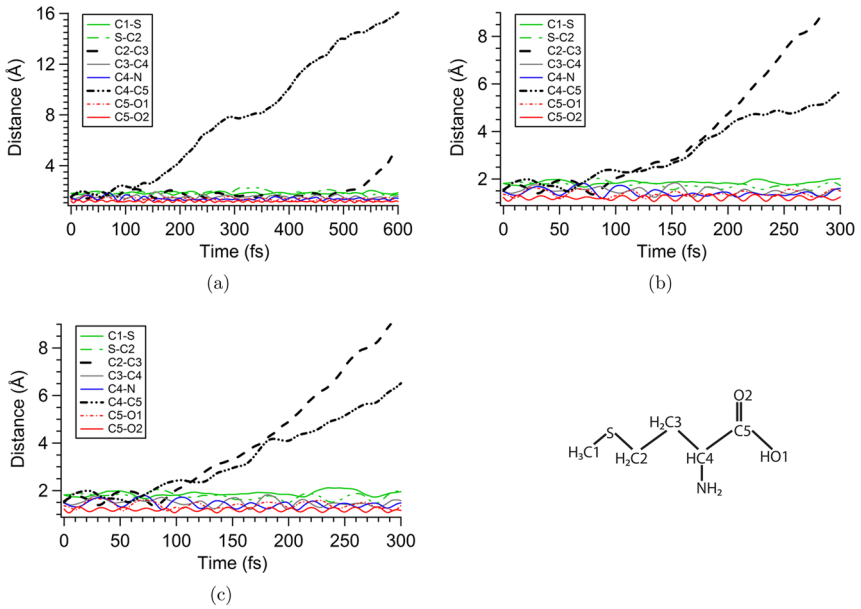

Figure 7. Bond lengths of doubly charged methionine in the CP MD simulations with initial temperatures of (a) T = 5773 K, (b) T = 6210 K, and (c) T = 6538 K. See legends in figure for further details.

dx.doi.org/10.1021/jp4113238 | J. Phys. Chem. A 2014, 118, 1374−1383

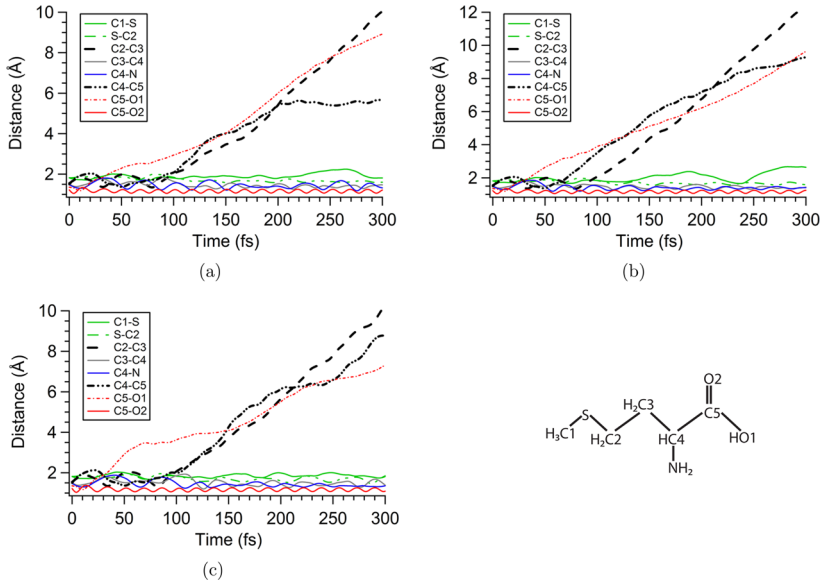

Figure 8. Bond lengths of doubly charged methionine in the CP MD simulations with initial temperatures of (a) T = 8072 K, (b) T = 8854 K, and (c) T = 10026 K.

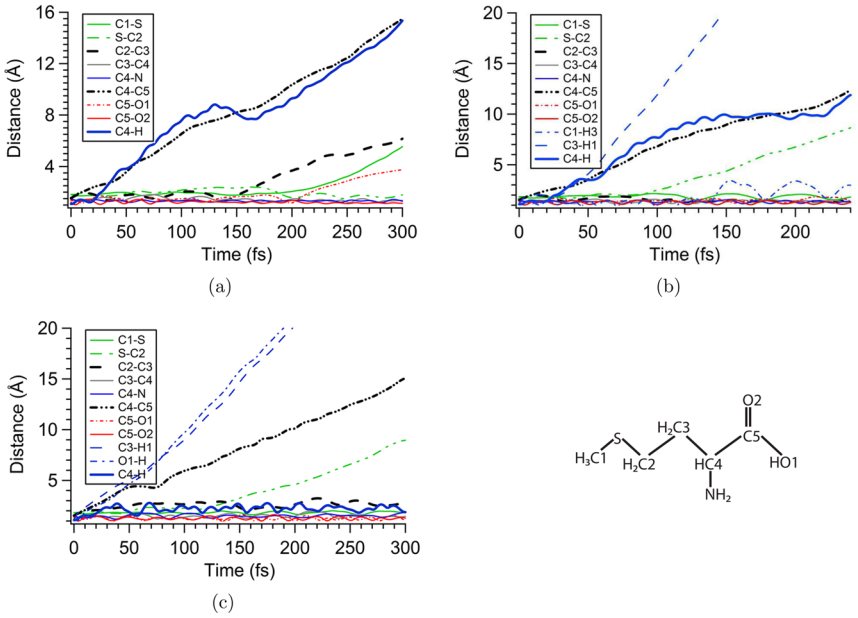

Figure 9. Bond lengths of doubly charged methionine in the CP MD simulations with initial temperatures of (a) T = 12174 K, (b) T = 13198 K, and (c) T = 15292 K.

has a strong yield at around 145 eV, indicating that this is the fragmentation channel that opens first, in the lowest energetic levels of the dicationic parent molecular states. This is consistent with the fact that the peak at m/z 61 is the most intense peak in the mass spectrum of singly ionized methionine[29] and indicates that $MeSCH_2^+$ is a good leaving group. Notably, there is no two-body channel observed, where the remaining molecules would remain intact after the carboxyl ion departure. Even for the lowest-energy doubly ionized states, there is always secondary bond breakage, first at the $-CH_2-CH_2-$ bond. On the other hand, the lighter fragment pairs are produced across the entire spectrum, albeit with more enhanced yields at lower energies corresponding to deeper vacancies. This rather state-insensitive behavior of the mentioned ion pairs may be in part caused by the assignment of a number of different actual fragmentation channels to these mass pairs (Table 1).

COMPUTATIONAL RESULTS

Molecular dynamics of doubly charged methionine with the initial temperatures based on the CP MD simulations always predicts C4−C5 bond breakage (Table 2). Typically, the C4−C5 bond scissoring occurs first in less than 150 fs (Figure 6) in the cases of low temperatures (3630, 4250, 4632, 5327, 5773, 6210, and 6358 K), resulting in the detachment of either a neutral or a charged carboxyl radical. At higher temperatures, the C4−C5 bond does not always break first. At the lowest temperatures (3630, 4250, 4632, and 5327 K), we do not see breakage of the C2−C3 bond during the 300 fs time propagation; however, we cannot exclude that this process

dx.doi.org/10.1021/jp4113238 | J. Phys. Chem. A 2014, 118, 1374−1383

might occur at a much longer time (from a few hundred femtoseconds to picoseconds), i.e., after the C4−C5 bond scissoring.

Bond length variations in the cases of temperatures (5773, 6210, and 6538 K) are shown in Figure 7a−c: following the C4−C5 bond breakage the C2−C3 bond always breaks at time stamps inversely proportional to initial temperatures. To be more precise, the C2−C3 bond scissoring occurs about 400 fs after the C4−C5 breakage in the case of T = 5773 K, about 20 fs after the C4−C5 breakage in the case of T = 6210 K and about less than 20 fs after the C4−C5 breakage in the case of T = 6538 K.

That is to say, the dissociation begins by the detaching of a neutral carboxyl radical after which the remaining doubly charged fragment decomposes further into two singly charged fragments $MeSCH_2^+$ (m/z 61) and $CH_2CHNH_2^+$ (m/z 43) (Table 2). These findings are consistent with the experimental results concerning the pattern at m/z pair (43,61) in Figure 2.

With initial temperatures T = 8072 K, T = 8854 K, and T = 10026 K (Figure 8a−c) dissociation channels always open by ejecting a neutral hydroxyl radical which is then followed by C4−C5 and C2−C3 bond scissoring at different timestamps in different cases. In all cases, the fragmentation ends up in producing cations $MeSCH_2^+$ (m/z 61) and $CH_2CHNH_2^+$ (m/z 43) together with neutral fragments CO and OH (also in Table 2). These findings are again consistent with the experimental results concerning the peak at m/z pair (43,61) in Figure 2.

With the highest temperatures (12174, 13198, 15292, 17786, and 19896 K), dissociation begins very early (at less than 20 fs) and also involves cutting multiple bonds. Hydrogen capture and some isomerization also occur in the dissociation processes. Parts a−c of Figure 9 plot bond lengths of the first three temperatures, and the related dissociation products are presented in Table 2. At the temperature of 15292 K, ultrafast fragmentation leads to cations MeS^+ and $CH_2(CH)_2NH_2^+$ and other neutral fragments. There are some indications in the experiment that such a very weak channel of the m/z pair (47,56) might exist, but not enough events were observed to be sure. At temperatures T = 12174 K and T = 13198 K the C4−C5 bond begins to break at around 10 fs, which is followed by hydrogen capture from C4 by the carboxyl radical. Some of the charged fragments predicted by the CP MD simulations at these high temperatures are not seen in the experiment. This is most likely due to our assumption that fragmentation arising from vacancies created in innermost orbitals can be simulated from ground-state doubly charged methionine by including temperature. A more careful analysis of these cases would require the use of TDDFT-EMD calculations, in which one can explicitly account for these vacancies as described, e.g., in ref 13.

CONCLUSIONS

The molecular dynamics of methionine followed by the initial removal of a S 2p electron resulting in fragmentation via specific fragmentation schemes have been studied in this work. On the basis of the experimental results, the photofragmentation of methionine can be explained consistently by one general scenario of nuclear dynamics: either neutral or charged carboxyl radical separates, with no indication of further dissociation if the radical carries charge; the remaining part of the molecule always dissociates further into fragments ranging in size from m/z 61 to m/z 15, and there is also the possibility of hydrogen loss or transfer accompanying these processes.

The intensity of various fragmentation channels depends on the electronic states of the parent dication in two very distinctly different ways: In the first case the heaviest fragment pairs ($CH_2CHNH_2^+$, $MeSCH_2^+$) and ($COOH^+$, $MeSCH_2^+$) are correlated mainly with the Auger electrons of high kinetic energy. These channels are thus open mainly for the electronic states with vacancies in weakly bound molecular orbitals. As they require the least amount of broken bonds, these channels are also least energy-consuming. However, no fragmentation channel with minimal damage (two-body process) was observed. In the second case, the lighter cation pairs are observed in coincidence with Auger electrons with the kinetic energy across the entire spectrum (127−151 eV), although the yields are stronger for higher-lying electronic states.

The above measurements have been complemented by ab initio CP MD calculations of doubly charged methionine in the ground state with various initial temperatures. The C4−C5 bond breakage is observed in all cases. In the lowest temperatures the C4−C5 bond breakage results in either a charged or a neutral carboxyl radical. Further dissociation in these cases may occur after a long time (possibly from a few hundred femtoseconds to picoseconds). At intermediate temperatures, singly charged carboxyl detachment is followed by C2−C3 bond cleavage resulting in fragments COOH (m/z 45), $CH_2CHNH_2^+$ (m/z 43), and $MeSCH_2^+$ (m/z 61). At the highest temperatures, fragmentation begins in less than 20 fs. The dissociation involves isomerization, hydrogen capture and loss.

It is notable that the sequence of fragmentation dynamics that emerged from the experiment is supported by the CP MD simulations; in both theory and experiment the separation of the carboxyl group always occurs, but the cationic fragment CO^+ is not observed. Also, the dissociation channel producing the fragments COOH (m/z 45), $CH_2CHNH_2^+$ (m/z 43), and $MeSCH_2^+$ (m/z 61) in the CP MD simulations is consistent with the experimental results concerning the m/z pair (43,61). Despite the incapability of describing molecular fragmentation starting from the high energy Auger final states by using the CP MD method, the procedure consisting of adding different amounts of extra energy in the CP MD simulations can reveal typical features of the dissociation dynamics of doubly charged methionine molecules such as ejection of a carboxyl group, fragmentation time scales, and opening of more complex dissociations at high energies.

AUTHOR INFORMATION

Corresponding Author

*D. T. Ha: e-mail, dangtrinh.ha@utu.fi.

Notes

The authors declare no competing financial interest.

ACKNOWLEDGMENTS

We thank the Väisälä Foundation, the Academy of Finland, the EU Transnational Access to Research Infrastructures program and the COST Action CM1024 (XLIC) for their financial support. We also acknowledge computer time from CCC-UAM, the Magerit CeSVima, and the Finnish Grid Infrastructure (FGI) project (Turku, Finland). The work is partially supported by the MICINN projects no. FIS2010-15127, CTQ2010-17006, and CSD2007-00010, and the CAM project S2009/MAT1726. M.A H. acknowledges funding from the Natural Science and Engineering Research Council of Canada

and the Canadian Space Agency. We thank the staff of MAX-lab for their help during the experiments. We are grateful to I. Tavernelli and P. López-Tarifa for useful discussions, and for practical guidance with the CPMD code.

REFERENCES

(1) Refsum, H.; Ueland, P. M.; Nygård, O.; Vollset, D. S. E. Homocysteine and Cardiovascular Disease. *Annu. Rev. Med.* **1998**, *49*, 31−62.
(2) Danby, C.; Eland, J. Photoelectron-Photoion Coincidence Spectroscopy: II. Design and Performance of a Practical Instrument. *Int. J. Mass Spectrom. Ion Phys.* **1972**, *8*, 153−161.
(3) Simon, M.; LeBrun, T.; Morin, P.; Lavollée, M.; Maréchal, J. L. A Photoelectron-Ion Multiple Coincidence Technique Applied to Core Ionization of Molecules. *Nucl. Instrum. Methods Phys. Res. B* **1991**, *62*, 167−174.
(4) Simon, M.; Morin, P.; Lablanquie, P.; Lavollée, M.; Ueda, K.; Kosugi, N. Dissociation Dynamics of Core-Excited BF3 Probed by the Photoelectron-Photoion-Photoion Coincidence. *Chem. Phys. Lett.* **1995**, *238*, 42−46.
(5) Field, T. A.; Eland, J. H. D. An Electron Ion Coincidence Spectrometer for Single and Double Photoionization Studies. *Meas. Sci. Technol.* **1998**, *9*, 922.
(6) Harada, C.; Tada, S.; Yamamoto, K.; Senba, Y.; Yoshida, H.; Hiraya, A.; Wada, S.; Tanaka, K.; Tabayashi, K. Dissociation Mechanisms and Dynamics of Doubly Charged CD3CN Observed by PEPIPICO Spectroscopy. *Radiat. Phys. Chem.* **2006**, *75*, 2085−2089.
(7) Yasunori, S.; Hiroaki, Y.; Keiichi, K.; Yoshinari, M.; Masaki, M.; Takayuki, M.; Tatsuo, G.; Kazuhiko, M.; Atsuya, H. Study on Dissociation Dynamics of Core-Excited Acetonitrile by Auger Electron-Photoion-Photoion Coincidence Measurements. *Bunshi Kozo Sogo Toronkai Koen Yoshishu* **2000**, *2000*, 74.
(8) Car, R.; Parrinello, M. Unified Approach for Molecular Dynamics and Density-Functional Theory. *Phys. Rev. Lett.* **1985**, *55*, 2471−2474.
(9) CPMD v. 3.15. Copyright IBM Corp 1990−2006, Copyright MPI für Festkörperforschung Stuttgart 1997−2001.
(10) Tavernelli, I.; Röhrig, U. F.; Rothlisberger, U. Molecular Dynamics in Electronically Excited States Using Time-Dependent Density Functional Theory. *Mol. Phys.* **2005**, *103*, 963−981.
(11) Tavernelli, I.; Gaigeot, M.-P.; Vuilleumier, R.; Stia, C.; Hervé du Penhoat, M.-A.; Politis, M.-F. Time-Dependent Density Functional Theory Molecular Dynamics Simulations of Liquid Water Radiolysis. *ChemPhysChem* **2008**, *9*, 2099−2103.
(12) Ndongmouo Taffoti, U. F.; Dinh, P. M.; Reinhard, P.-G.; Suraud, E.; Wang, Z. P. Exploration of Dynamical Regimes of Irradiated Small Protonated Water Clusters. *Eur. Phys. J. D* **2010**, *58*, 131−136.
(13) López-Tarifa, P.; Hervé du Penhoat, M.-A.; Vuilleumier, R.; Gaigeot, M.-P.; Tavernelli, I.; Le Padellec, A.; Champeaux, J.-P.; Alcamí, M.; Moretto-Capelle, P.; Martín, F.; Politis, M.-F.; et al. Ultrafast Nonadiabatic Fragmentation Dynamics of Doubly Charged Uracil in a Gas Phase. *Phys. Rev. Lett.* **2011**, *107*, 023202.
(14) López-Tarifa, P. Fragmentation Dynamics of Biomolecules in Gas Phase and Water Environment. *Ph.D. Thesis*, Universidad Autónoma de Madrid, 2011.
(15) Frisch, M. J.; Trucks, G. W.; Schlegel, H. B.; Scuseria, G. E.; Robb, M. A.; Cheeseman, J. R.; Montgomery, J. A., Jr.; Vreven, T.; Kudin, K. N.; Burant, J. C.; et al. *Gaussian 03*, Revision C.02; Gaussian, Inc.: Wallingford, CT, 2004.
(16) Kleinman, L.; Bylander, D. M. Efficacious Form for Model Pseudopotentials. *Phys. Rev. Lett.* **1982**, *48*, 1425−1428.
(17) Tang, W.; Sanville, E.; Henkelman, G. A Grid-Based Bader Analysis Algorithm Without Lattice Bias. *J. Phys.: Condens. Matter* **2009**, *21*, 084204.
(18) Arnaldsson, A.; Tang, W.; Chill, S.; Henkelman, G. *Bader Charge Analysis Code*.
(19) Bässler, M.; Ausmees, A.; Jurvansuu, M.; Feifel, R.; Forsell, J.-O.; de Tarso Fonseca, P.; Kivimäki, A.; Sundin, S.; Sorensen, S.; Nyholm, R.; et al. Beam Line I411 at MAX II - Performance and First Results. *Nucl. Instrum. Methods Phys. Res. A* **2001**, *469*, 382−393.
(20) Kukk, E.; Sankari, R.; Huttula, M.; Sankari, A.; Aksela, H.; Aksela, S. New Electron-Ion Coincidence Setup: Fragmentation of Acetonitrile Following N 1s Core Excitation. *J. Electron. Spectrosc. Relat. Phenom.* **2007**, *155*, 141−147.
(21) Huttula, M.; Heinäsmäki, S.; Aksela, H.; Kukk, E.; Aksela, S. Multielectron Effects in 4p Photoionization of Atomic Cs. *J. Electron Spectrosc. Relat. Phenom.* **2007**, *156−158*, 270−273.
(22) Kukk, E. *PEPIPICO analysis toolkit*.
(23) Eland, J. H. D. Dynamics of Fragmentation Reactions From Peak Shapes in Multiparticle Coincidence Experiments. *Laser Chem.* **1991**, *11*, 259−263.
(24) Itälä, E.; Ha, D. T.; Kooser, K.; Rachlew, E.; Huels, M. A.; Kukk, E. Fragmentation Patterns of Core-Ionized Thymine and 5-bromouracil. *J. Chem. Phys.* **2010**, *133*, 154316.
(25) Ha, D. T.; Huels, M. A.; Huttula, M.; Urpelainen, S.; Kukk, E. Experimental and *Ab Initio* Study of the Photofragmentation of DNA and RNA Sugars. *Phys. Rev. A* **2011**, *84*, 033419.
(26) Itälä, E.; Ha, D.; Kooser, K.; ommiste, E. N.; Joost, U.; Kukk, E. Fragmentation Patterns of Core Ionized Uracil. *Int. J. Mass Spectrom.* **2011**, *306*, 82−90.
(27) Gil, A.; Simon, S.; Rodríguez-Santiago, L.; Bertrán, J.; Sodupe, M. Influence of the Side Chain in the Structure and Fragmentation of Amino Acids Radical Cations. *J. Chem. Theory Comput.* **2007**, *3*, 2210−2220.
(28) Capron, M.; Díaz-Tendero, S.; Maclot, S.; Domaracka, A.; Lattouf, E.; Lawicki, A.; Maisonny, R.; Chesnel, J.-Y.; Méry, A.; Poully, J.-C.; et al. A Multicoincidence Study of Fragmentation Dynamics in Collision of ?-Aminobutyric Acid with Low-Energy Ions. *Chem.—Eur. J.* **2012**, *18*, 9321−9332.
(29) NIST Chemistry WebBook - Mass Spectrum of Methionine. http://webbook.nist.gov/cgi/cbook.cgi?ID=C63683&Units=SI Mask=200#Mass-Spec.